

Analytical Second Derivatives for Effective Core Potential. Application to Transition Structures of $\text{Cp}_2\text{Ru}_2(\mu\text{-H})_4$ and to the Mechanism of Reaction $\text{Cu} + \text{CH}_2\text{N}_2$

Qiang Cui, Djameladdin G. Musaev, Mats Svensson, and Keiji Morokuma*

Cherry L. Emerson Center for Scientific Computation and Department of Chemistry, Emory University, Atlanta, Georgia 30322

Received: February 22, 1996; In Final Form: April 13, 1996[⊗]

Routines for calculation of analytical second derivatives for the effective core potential have been developed. The present version allows for spdf basis sets with spdfg projection operators for HF, DFT, and MP2 methods and has been incorporated into the Gaussian package. Analytical frequency analysis has been applied to the characterization of a critical structure of $\text{Cp}_2\text{Ru}_2(\mu\text{-H})_4$ and to the study of the mechanism of reaction between Cu and CH_2N_2 . Frequency analysis demonstrates that the structure previously found as the transition state of H_2 dissociation of $\text{Cp}_2\text{Ru}_2(\mu\text{-H})_4$ actually is a third-order stationary point. For various species of the system of $\text{Cu} + \text{CH}_2\text{N}_2$, DFT and MP2 second derivatives gave reasonable frequencies ($\sim 5\%$ average error) compared to the experimental in most cases, except that the N–N stretch was very poor at the MP2 level because of spin contamination in N_2CuCH_2 . On the basis of vibrational frequencies, assignment has been made for adducts found experimentally between Cu and CH_2N_2 . The energetics was also studied with the PCI-80 method and compared with DFT and *ab initio* results. The best estimated binding energy for $\text{Cu}-\text{CH}_2$ is 60.8 kcal/mol. The end-on isomer is the only stable $\text{N}_2\cdot\text{CuCH}_2$ species, and the side-on $\text{N}_2\cdot\text{CuCH}_2$ isomerizes to the end-on form without barrier. The best estimate of binding energy for N_2-CuCH_2 is 19.4 kcal/mol for the end-on complex. The overall reaction for $\text{Cu} + \text{CH}_2\text{N}_2 \rightarrow \text{CuCH}_2 + \text{N}_2$ is 34.9 kcal/mol exothermic. The reaction is found to take place without substantial barrier. The effect of recontraction of the ECP-associated basis set in DFT calculations is also briefly discussed.

I. Introduction

It is well-known that the effective core potential (ECP)^{1,2} provides an efficient method for *ab initio* calculation of systems containing heavy elements. ECP is also the only practical method for taking into account the relativistic effects for polyatomic molecules. Frequency analysis, based on analytical second derivatives of energy, is widely used for calculation of vibrational spectra and zero-point energy and entropy as well as for search and characterization of equilibrium and transition state structures. Though routines for Hartree–Fock analytical second derivatives for ECP (up to d Gaussian basis functions) have been reported by Komornicki et al.,³ the lack of a widely available analytical second-derivative package has been one of the stumbling blocks for a convenient use of ECPs. While the present paper is being finalized, the Hartree–Fock analytical second derivative with ECP is implemented in the MESA program.⁴

In the present paper, we have developed the routines for calculation of analytical second derivatives for ECP and incorporated them into the Gaussian package.⁵ The present version allows for spdf Gaussian basis functions and spdfg projectors for Hartree–Fock (HF), density functional theory (DFT), and second-order Møller–Plesset perturbation (MP2) calculations. In the next section, we first present the method used for implementation. The method was then used for characterization of a “transition state” structure for $\text{CpRu}(\mu\text{-H})_4\text{RuCp}$. In the following section, we have applied the method for elucidation of the mechanism of reaction $\text{Cu} + \text{CH}_2\text{N}_2$, which is followed by brief concluding remarks.

II. ECP Analytical Second Derivatives

In the ECP method, the potential due to core electrons is replaced by the effective core potential usually in the following

form¹

$$U_C(r) = U_C^{L+1}(r) + \sum_{l=0}^L \sum_{m=-l}^l |lm\rangle [U_C^l(r) - U_C^{L+1}(r)] \langle lm| \quad (1)$$

$$r_c^2 \left[U_C^{L+1}(r) - \frac{N_c}{r_c} \right] = \sum_j d_{jl} [r_c^{n_j} \exp(-\xi_j r_c^2)] \quad (2)$$

$$r_c^2 [U_C^l(r) - U_C^{L+1}(r)] = \sum_j d_{jl} [r_c^{n_j} \exp(-\xi_j r_c^2)] \quad (3)$$

where L is the largest angular momentum appearing in the core. The total ECP is the sum of $U_C(r)$ over heavy atoms:

$$U(r) = \sum_C U_C(r) \quad (4)$$

The calculation of the second derivative of the ECP total energy formally requires not only the derivatives of normal integrals and densities but also the derivatives of ECP integrals $\partial^2/(\partial X_A \partial Y_B) \langle \phi_\mu^I | U | \phi_\nu^J \rangle$, where X_A and Y_B are Cartesian coordinates of atom A and B, respectively, and ϕ_μ^I and ϕ_ν^J are basis functions on atoms I and J, respectively. Since the form of the ECPs is rather complicated, it is advantageous to replace the derivatives of the ECPs themselves by derivatives of basis functions by using the principle of translational invariance.² For the second derivatives, for instance

$$\begin{aligned} \left\langle \phi_\mu^I \left| \frac{\partial^2 U}{\partial X_A \partial Y_B} \right| \phi_\nu^J \right\rangle &= \{ \langle \partial^2 \phi_\mu^I / \partial X_I \partial Y_I | U_A | \phi_\nu^J \rangle + \\ &\langle \phi_\mu^I | U_A | \partial^2 \phi_\nu^J / \partial X_J \partial Y_J \rangle + \langle \partial \phi_\mu^I / \partial X_I | U_A | \partial \phi_\nu^J / \partial Y_J \rangle + \\ &\langle \partial \phi_\mu^I / \partial Y_I | U_A | \partial \phi_\nu^J / \partial X_J \rangle \} \delta_{AB} \quad (5) \end{aligned}$$

[⊗] Abstract published in *Advance ACS Abstracts*, June 1, 1996.

Then, after some simple algebraic manipulation, the second derivatives of ECP integrals are reduced into the form below:

$$\begin{aligned} \frac{\partial^2}{\partial X_A \partial Y_B} \langle \phi_\mu^I | U | \phi_\nu^J \rangle = & \langle \partial^2 \phi_\mu^I / \partial X_I \partial Y_I | U \delta_{AI} \delta_{BI} - U_B \delta_{AI} - U_A \delta_{BI} + U_A \delta_{AB} | \phi_\nu^J \rangle + \\ & \langle \phi_\mu^I | U \delta_{AJ} \delta_{BJ} - U_B \delta_{AJ} - U_A \delta_{BJ} + U_A \delta_{AB} | \partial^2 \phi_\nu^J / \partial X_J \partial Y_J \rangle + \\ & \langle \partial \phi_\mu^I / \partial X_I | U \delta_{AI} \delta_{BJ} - U_B \delta_{AI} - U_A \delta_{BJ} + U_A \delta_{AB} | \partial \phi_\nu^J / \partial Y_J \rangle + \\ & \langle \partial \phi_\mu^I / \partial Y_I | U \delta_{AJ} \delta_{BI} - U_B \delta_{AJ} - U_A \delta_{BI} + U_A \delta_{AB} | \partial \phi_\nu^J / \partial X_J \rangle \quad (6) \end{aligned}$$

The ECP contribution to the energy second derivative is thus

$$\begin{aligned} \frac{\partial^2 E_{\text{ECP}}}{\partial X_A \partial Y_B} = 2 \sum_\mu \sum_\nu P_{\mu\nu} \langle \langle \partial^2 \phi_\mu^I / \partial X_I \partial Y_I | U \delta_{AI} \delta_{BI} - U_B \delta_{AI} - \\ U_A \delta_{BI} + U_A \delta_{AB} | \phi_\nu^J \rangle + \langle \partial \phi_\mu^I / \partial X_I | U \delta_{AI} \delta_{BJ} - U_B \delta_{AI} - \\ U_A \delta_{BJ} + U_A \delta_{AB} | \partial \phi_\nu^J / \partial Y_J \rangle \rangle \quad (7) \end{aligned}$$

It is well-known that the derivatives of Gaussian type primitives are just linear combinations of primitives with different angular momenta:

$$\phi_{l,m,n} = N_{lmr} x_A^l y_A^m z_A^n e^{-\alpha_A |r-R_A|^2}$$

$$\frac{\partial^2 \phi_{l,m,n}}{\partial X_A^2} \propto l(l-1)\phi_{l-2,m,n} - 2\alpha(2l+1)\phi_{l,m,n} + 4\alpha^2\phi_{l+2,m,n}$$

$$\frac{\partial^2 \phi_{l,m,n}}{\partial X_A \partial Y_A} \propto ml\phi_{l-1,m-1,n} - 2\alpha m\phi_{l+1,m-1,n} - 2\alpha l\phi_{l-1,m+1,n} + 4\alpha^2\phi_{l+1,m+1,n}$$

For example, the second derivative of an f function is just a linear combination of p, f, and h functions with certain coefficients. Here the symbol indicates that normalization coefficients are considered separately for convenience in the program. Thus the derivatives of normal ECP integrals with Gaussian primitives are further reduced into the combination of normal ECP integrals. For example:

$$\begin{aligned} \langle \partial^2 f_{x^3} / \partial X_A^2 | U_C | \phi_\nu^J \rangle \propto \\ 6\langle p_x | U_C | \phi_\nu^J \rangle - 14\alpha \langle f_{x^3} | U_C | \phi_\nu^J \rangle + 4\alpha^2 \langle h_{x^5} | U_C | \phi_\nu^J \rangle \end{aligned}$$

The Gaussian package is capable of calculating analytical gradients for ECP integrals, equipped with the ECP program written by R. L. Martin.⁵ Though his routine for collecting terms for ECP second derivatives is also included, the contribution of first derivatives of ECP integrals is not considered in the gradient of the Fock matrix, which is required in the calculation of the second derivative of the total energy. We followed the existing mechanism for normal second derivatives and developed routines giving analytical force constants for ECP. In order to calculate the second derivatives for f basis functions, we need to evaluate ECP integrals for h basis functions. Martin's ECP integral routine in Gaussian92/DFT and Gaussian 94 can calculate only up to f basis functions. According to McMurchie and Davidson,⁶ we only need to extend the table for spherical harmonics to higher l values. We took such a table for g basis functions developed by H. J. Flad and H. Stoll⁷ in connection with R. S. Pitzers' ECP program⁸ and extended the table to h basis functions for spherical harmonics of l = 9, 10 with a slightly different method.

If an *ab initio* program has the capability of calculating analytical second derivatives for non-ECP calculations, incorporation of the routines for the ECP analytical second derivatives is not difficult using the clear ideas discussed above. Though the present version can only handle Hartree–Fock, density-functional, and MP2 methods, we hope to extend to other methods such as CASSCF.

III. Characterization of a “Transition State” Structure for CpRu(μ -H)₄RuCp

The present program was applied to a large system, CpRu(μ -H)₄RuCp where Cp = C₅H₅, in order to examine the power of the analytical ECP second derivatives. Using only the gradient of ECP, Koga and Morokuma (KM) determined the “transition state” for H₂ dissociation from the stable complex CpRu(μ -H)₄RuCp.⁹ We have reoptimized the structure and obtained the same result, as shown in Figure 1a, using the same approximation, i.e. the RHF method with the standard Lan11DZ basis set with the Hay–Wadt valence electron ECP for Ru,^{1g} assuming the overall C_{2v} symmetry with local C_{5v} for Cp rings. An analytical frequency analysis took nearly 15 h on an IBM RS/6000 Model 350. Numerical differentiation of the gradient for this system of large number (21) of degrees of freedom would have taken about 100 h on the same machine. Unable to perform such a calculation, KM assumed that the transition state optimized under C_{2v} constraint is the true transition state.

For KM's “transition structure” we found *three* imaginary frequencies, with corresponding normal modes shown in Figure 1b–d. The largest imaginary frequency, 1072.5i cm⁻¹, belongs to a₁ and, as seen in Figure 1b, clearly represents the true reaction coordinate for dissociation of H₂. The next one, 434.2i cm⁻¹, in b₂ in Figure 1c, shows that the true transition state wants to distort from C_{2v} to C_s symmetry, making the four hydrogen bridge bonds nonsymmetric. KM also found for the reactant complex CpRu(μ -H)₄RuCp that the symmetrically hydrogen-bridged structure is slightly higher in energy than the nonsymmetrically hydrogen-bridged structure at the RHF level; when electron correlation is taken into account at the MP2 level the symmetric structure becomes lower in energy than the nonsymmetric structure. The smallest imaginary frequency, 133.2i cm⁻¹, in Figure 1d corresponds to the rotation of four bridged hydrogens within the xz symmetry plane. This can also be regarded as the rotation of the Cp rings; apparently the dissociating hydrogen molecule H¹H² (atomic labels in Figure 1a) does not want to be on top of one of the Cp ring carbon atoms. However, since the two extra imaginary frequencies are small, KM's conclusions based on the C_{2v} “transition state” seem to be unaffected. The successful application of the program and the timing data suggest that the analytical second derivative will have a large impact on geometry optimization, characterization, assignment of vibrational spectra, and zero-point energy evaluation of large organometallic systems.

IV. Mechanism of Reaction Cu + CH₂N₂

By using the ECP analytical second derivative extensively, we have studied the potential energy surface for the ground state reaction of Cu + N₂CH₂. This reaction was studied in detail by Chang et al. via FTIR matrix isolation spectroscopy.¹⁰ It has been found that the copper atom inserts easily into the CN bond of diazomethane in argon matrices at 12 K, leading to a carbene complex of copper, CuCH₂, **1**, and an N₂ molecule. Several intermediates such as dinitrogen–copper–methylene complex, N₂CuCH₂, and Cu(CH₂N₂) have been identified as well. However, the mechanism of this reaction as well as the structure and stability of the observed intermediates still remains

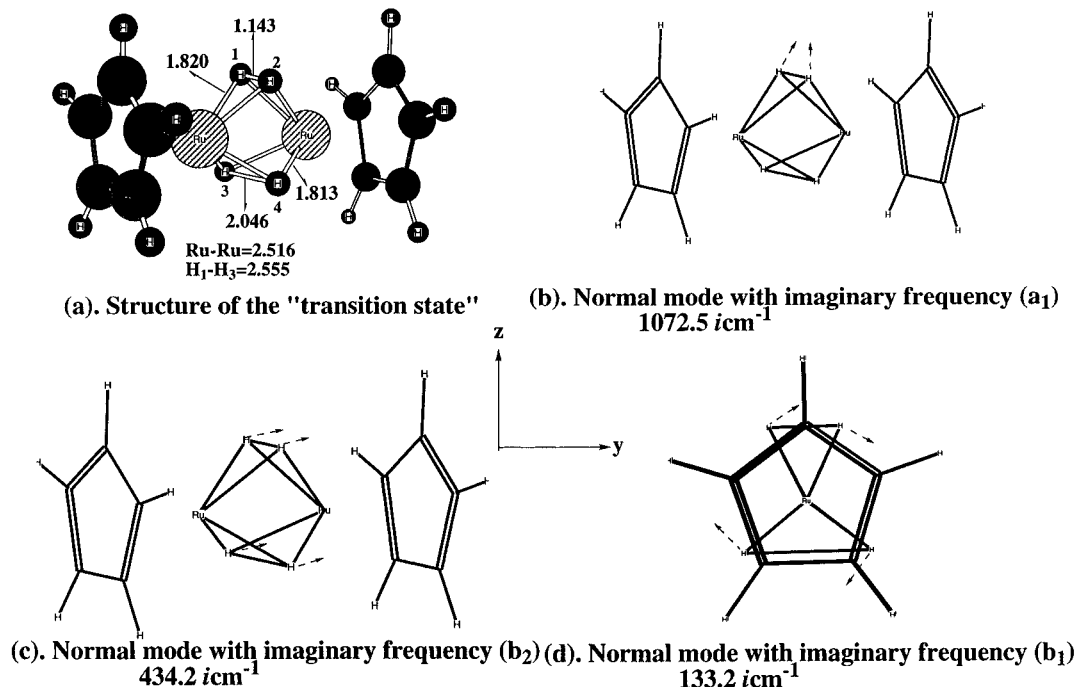
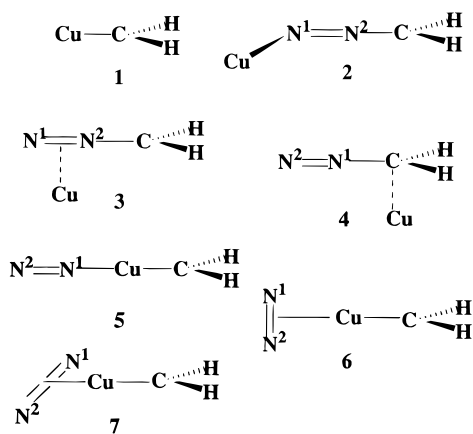


Figure 1. Structure and normal modes (RHF/Lan11dz) of the transition state for H_2 dissociation in the $Cp_2Ru_2(\mu-H)_4$ complex.

unclear. In order to solve these problems we have applied the Gaussian-92/DFT programs with the newly implemented ECP analytical second-derivative code to study the potential energy surface of the ground state reaction



It is well-known that the ground state of copper atom is 2S (sd^{10}) with the 2D (s^2d^9) state 1.49 eV higher in energy.¹¹ According to a previous study, the global minimum of diazomethane CH_2N_2 has end-on coordination of N_2 to the CH_2 fragment.¹² The three-membered ring isomer, diazirine, is calculated to be 6.5 kcal/mol higher. Therefore, we decided to study only the reaction 8 of Cu (2S , sd^{10}) with diazomethane.



In these calculations we have used the UHF and UMP2 levels of theory to optimize geometries. For comparison, we also optimized geometries with the DFT method using the Becke¹³ or the Becke three-parameter¹⁴ nonlocal exchange functional together with the Lee-Yang-Parr nonlocal correlation functional,¹⁵ BLYP or B3LYP. The single- and double-excitation coupled cluster method with a perturbational triple correction, CCSD(T), energies were evaluated at DFT-optimized geometries and compared with DFT and other energies. In order to obtain even better estimates of relative energies, PCI-80¹⁶ single-point

calculations were carried out at B3LYP-optimized geometries. In the PCI-80 method correlation effects from an MCPF¹⁷ calculation are extrapolated by simply adding 20% of the calculated correlation energy.¹⁶

Two basis sets were used in the geometry optimization. Basis I is the standard Lan12DZ basis set, which includes the nonrelativistic Hay-Wadt 19-valence electron ECP with a valence double ζ basis set for Cu^{18} and a double ζ basis set for C, N, and H.^{18a} In basis set II the same ECP basis was used for Cu and the polarization 6-31G(d,p) set for C, N, and H.^{18b-d} All CCSD(T) energies were calculated using the basis set II. PCI-80 calculations were performed without ECP using a large all-electron basis set, which we refer to as basis set III, and relativistic effects were added using perturbation theory for the mass-velocity and Darwin terms.¹⁶

There has been some concern about the appropriateness of using the Hay-Wadt effective core potentials along with their associated valence basis sets in DFT calculations. In order to examine the issue for the case of Cu, we also performed some calculations for $CuCH_2$ using DFT contraction of Hay-Wadt primitives in basis set I, which will be discussed in detail in section E.

The optimized structures of the reactant $Cu + CH_2N_2$, the reactant complex $Cu(N_2CH_2)$, the transition states, and the products $N_2 + CuCH_2$ were positively identified as local minima and saddle points through normal coordinate analysis with the analytical second derivatives. Their geometries are shown in Figure 2 and Table 1, and energies are shown in Table 2.

A. Structure of Adduct Complex $Cu(CH_2N_2)$. It is natural to expect that the first step of the reaction is coordination of N_2CH_2 to Cu atom to form the adduct complex $Cu(CH_2N_2)$, which has been detected experimentally. Three possible structures, 2-4, corresponding to the coordination of copper atom at the end-on and side-on sites of nitrogen and the carbon site, respectively, are suggested.

Before examining these structures, it is instructive to study the CuN_2 molecule. The interaction between the copper atom and nitrogen is very weak, and therefore the structure of the complex is sensitive to the level of calculation, as shown in Table 1. Neither the side-on nor the end-on CuN_2 complex is

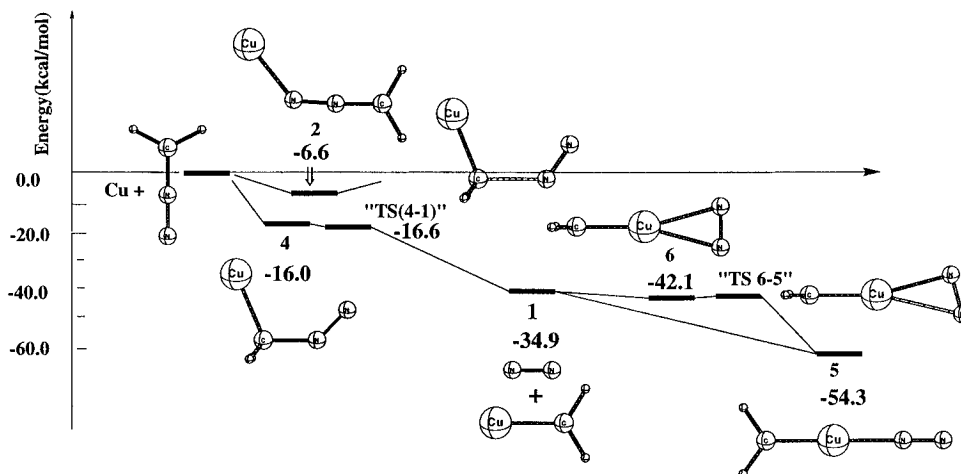


Figure 2. Potential energy surface for the system of Cu + CH₂N₂ at the level of PCI-80/III/B3LYP/II+ZPE+relativistic effect.

TABLE 1: *Ab Initio* and DFT Geometrical Parameters (in Å and deg) of Intermediates and Transition States for the Reaction System Cu + CH₂N₂ with the Basis Set II^a

compound	method	geometrical parameters					γ^b
		C-N	C-H	H-C-N	N-N		
CH ₂ N ₂	BLYP	1.304	1.087	118.2	1.161		0.0(C _{2v})
C _s	B3LYP	1.294	1.080	118.1	1.146		0.0(C _{2v})
	MP2	1.315	1.074	116.2	1.151		18.5
Cu•N ₂	B3LYP	Cu-N	N-N	Cu-N-N			
		2.223	1.113	136.5			
C _s	MP2	3.456	1.131	149.5			
² B ₁ CuCH ₂ (1)	BLYP	Cu-C	C-H	Cu-C-H			
	B3LYP	1.846	1.095	121.1			
	MP2	1.857	1.089	121.9			
end-on Cu•NNCH ₂ (2)	BLYP	Cu-N ¹	C-N ²	N ¹ -N ² -C	Cu-N ¹ -N ²		N ¹ -N ²
	B3LYP	1.925	1.294	175.5	134.6		1.190
	MP2	1.961	1.282	174.8	134.2		1.173
C _s , planar	B3LYP	2.118	1.246	179.6	159.4		1.143
	MP2						
C-on Cu•NNCH ₂ (4)	BLYP	Cu-C	C-N ¹	N ² -N ¹ -C	Cu-C-N ¹		N ¹ -N ²
	B3LYP	1.960	1.469	142.1	115.0		1.169
	MP2	1.954	1.479	134.8	112.6		1.163
T.S. (4-1)	B3LYP	1.966	1.484	135.5	106.0		1.150
	BLYP	1.898	1.878	126.2	113.7		1.147
	B3LYP	1.905	1.869	123.9	112.0		1.136
C _s	MP2	1.925	1.821	127.2	108.1		1.122
end-on N ₂ •CuCH ₂ (5)	BLYP	Cu-C	C-H	Cu-C-H	Cu-N ¹		N ¹ -N ²
	B3LYP	1.854	1.099	124.1	1.894		1.129
	MP2	1.857	1.092	124.2	1.916		1.110
C _{2v}	B3LYP	1.905	1.104	124.1	1.918		1.109
	MP2						
T.S. (6-5) C _s	MP2	1.874	1.086	124.3	2.385/2.134		1.140
side-on N ₂ •CuCH ₂ (6)	BLYP	1.855	1.098	123.7	2.108		1.141
	B3LYP	1.861	1.091	123.8	2.143		1.120
	MP2	1.871	1.086	124.3	2.200		1.140
C _{2v} , perpendicular							
side-on N ₂ •CuCH ₂ (7)	BLYP	1.867	1.097	123.1	2.173		1.131
	B3LYP	1.871	1.091	123.3	2.206		1.114
	MP2	1.876	1.086	124.2	2.260		1.140
C _{2v} , planar							

^a The N-N distances in free N₂ are 1.118, 1.106, and 1.131 Å for BLYP, B3LYP, and MP2, respectively. ^b The angle between the HCH plane and the CN bond.

a local minimum; the equilibrium structure is bent with the Cu-N-N angle of 136.5° at the B3LYP/II level. It is weakly bound with a binding energy of 1.44 kcal/mol. At the MP2 level, the interaction is even weaker with the binding energy of 0.96 kcal/mol, and the Cu-N bond is much longer (3.46 Å) than the B3LYP optimized one (2.23 Å). PCI-80/III at the B3LYP/II optimized geometry gives the binding energy of 1.01 kcal/mol.

As shown in Table 1, Cu(N₂CH₂) **2** converged to a planar structure which is similar to that of the CuN₂ complex. The Cu-N distance, 1.96 Å (B3LYP/II), is shorter than in CuN₂,

indicating stronger interaction. The MP2/II optimized structure is rather different from the DFT results as in the case of CuN₂. Table 2 shows that the adduct **2** lies -9.3 and -14.5 kcal/mol relative to the reactants at the B3LYP/II and BLYP/II levels, respectively, and +1.7 kcal/mol at the MP2/II level. Inclusion of more correlation effect using the CCSD(T)/II/B3LYP/II and PCI-80/III/B3LYP/II approximation gives -2.1 and -7.4 kcal/mol, respectively. The stronger interaction of Cu with N₂CH₂ than with N₂ is also clearly indicated by the Mulliken population analysis in Table 3. The Cu-N overlap population of 0.18 in

TABLE 2: *Ab Initio*, DFT, and PCI-80 Total and Relative Energies of Intermediates and Transition States of the Reaction System Cu + CH₂N₂^a

compound	energetic parameters					
	BLYP/II	B3LYP/II	MP2/II	CCSD(T)/II//B3LYP/II	PCI-80/III//B3LYP/II+Rel ^b	PCI-80/III+Rel+ZPE ^c
³ S Cu + ³ B ₁ CH ₂	-235.1895	-235.2703	-234.1852	-234.1896	-1692.2850	-1692.3024
² B ₁ CuCH ₂ (1)	-70.4	-63.7	-47.6	-52.8	-63.7	-61.4
² S Cu + CH ₂ N ₂	-344.7696	-344.8555	-343.4809	-343.4976	-1801.7389	-1801.7709
end-on Cu·NNCH ₂ (2)	-14.5	-9.3	+1.7	-2.1	-7.4	-7.1
C-on Cu·NNCH ₂ (4)	-20.1	-16.7	-4.1	-11.4	-16.9	-16.5
T.S. (4-1)	-15.2	-10.7	+2.2	-8.5	-15.5	-17.1
end-on N ₂ ·CuCH ₂ (5)	-44.7/-20.2 ^d	-40.8/-17.6	-49.2/-20.1	-47.2/-19.0	-52.3/-20.3	-54.8/-19.4
T.S. (6-5)			-34.5/-6.4			
side-on N ₂ ·CuCH ₂ (6)	-33.3/-8.7	-29.9/-6.7	-35.1/-7.0	-33.8/-5.6	-40.3/-8.3	-42.6/-7.2
side-on N ₂ ·CuCH ₂ (7)	-30.0/-5.4	-28.1/-5.0	-34.4/-6.3	-33.1/-4.8	-39.0/-7.0	-41.5/-6.1
N ₂ + CuCH ₂ (1)	-26.8	-25.4	-27.3	-27.7	-32.0	-35.4

^a The total energies (in hartrees) are given only for reference structures, and the relative energies (in kcal/mol) are relative to the reference structures. ^b Corrected with the relativistic effect. ^c Zero-point energies are calculated with B3LYP/II. ^d After slash in italic, relative to N₂ + ²B₁ CuCH₂.

TABLE 3: Mulliken Population Analysis for CuCH₂, N₂·CuCH₂, and Cu·NNCH₂ at the B3LYP/II Level

	² B ₁ CuCH ₂ 1	end-on Cu·NNCH ₂ 2	C-on Cu·NNCH ₂ 4	end-on N ₂ ·CuCH ₂ 5	side-on N ₂ ·CuCH ₂ 6
gross orbital population on copper atom	(3p4p) ^{6.16} (3s4s) ^{2.87} 3d ^{9.80}	(3p4p) ^{6.19} (3s4s) ^{2.79} 3d ^{9.86}	(3s3p) ^{6.09} (3s4s) ^{2.96} 3d ^{9.85}	(3p4p) ^{6.20} (3s4s) ^{2.82} 3d ^{9.72}	(3p4p) ^{6.27} (3s4s) ^{2.78} 3d ^{9.76}
atomic charge	Cu	Cu	Cu	Cu	Cu
	+0.17	+0.09	+0.10	+0.26	+0.19
	C	C	C	C	C
	-0.40 (-0.26) ^a	-0.22 (-0.23) ^b	-0.30	-0.47	-0.44
	H	H	H	H	H
	+0.12 (+0.13)	+0.13 (+0.15)	+0.15	+0.10	+0.10
	N ¹	N ¹	N ¹	N ¹	N ¹
		-0.30 (-0.22)	-0.03	+0.02	+0.01
	N ²	N ²	N ²	N ²	N ²
		+0.15 (+0.16)	-0.10	-0.02	+0.01
overlap population	Cu-C	Cu-C	Cu-C	Cu-C	Cu-C
	0.41	0.01	0.28	0.40	0.41
	Cu-N ¹	Cu-N ¹	Cu-N ¹	Cu-N ¹	Cu-N ¹
		0.18 [0.08] ^c	0.03	0.09	0.06
	N ¹ -N ²	N ¹ -N ²	N ¹ -N ²	N ¹ -N ²	N ¹ -N ²
		0.42 (0.52) [0.58]	0.51	0.70	0.46
atomic spin density	Cu	Cu	Cu	Cu	Cu
	0.06	+0.73 [+0.90]	+0.26	+0.09	+0.07
	C	C	C	C	C
	+1.02 (+2.10)	-0.04	+0.04	+0.94	+0.94
	H	H	H	H	H
	-0.04 (-0.05)	+0.01	-0.00	-0.04	-0.04
	N ¹	N ¹	N ¹	N ¹	N ¹
		+0.12	+0.13	0.00	+0.04
	N ²	N ²	N ²	N ²	N ²
		+0.16	+0.56	+0.05	+0.04

^a Numbers in parentheses are for CH₂(³B₁). ^b Numbers in parentheses are for CH₂N₂. ^c Numbers in brackets are for CuN₂.

adduct **2** is considerably larger than that of 0.08 in CuN₂. On the other hand, the N-N overlap population of 0.42 is smaller than that of 0.58 in CuN₂, indicating a much weakened N-N bond.

There is no local minimum on the PES corresponding to the proposed side-on adduct **3**. Without any symmetry constraints it either converges to the adduct **2** or to the adduct **4** which has C_s symmetry. The C-N bond, 1.48 Å (B3LYP/II), is much stretched in adduct **4**, compared with that, 1.29 Å, in the reactant CH₂N₂, while the N-N distance remains nearly the same. The Cu-C distance is calculated to be 1.95 Å. The Cu-C-N bond angle of 112.6° and C-N-N bond angle of 134.8° indicate that the carbon atom has an sp³ and the nitrogen atom has an sp² hybridization. The fact that N-N-C-Cu prefers a cis-conformation indicates that there is some weak interaction between the Cu atom and the N-N group. The Mulliken population analysis in Table 3 shows that the unpaired electron in **4** is on the N² atom, consistent with the bonding picture mentioned above. Adduct **4** lies 16.7, 20.1, 4.1, and 11.4 kcal/mol below the reactants at the B3LYP/II, BLYP/II, MP2/II, and CCSD(T)/II//B3LYP/II levels, respectively. With PCI-80/III//B3LYP/II, the binding energy of Cu-N₂CH₂ is calculated to be 15.5 kcal/mol, not far from the CCSD(T) and B3LYP values. The transition state search for direct conversion between two structures of the complex Cu(N₂CH₂), **2** and **4**, always converged to the dissociation limit Cu + N₂CH₂. The only way of conversion is dissociation and recombination of Cu and N₂CH₂.

A search for transition states from the adduct **4** located a saddle point **TS(4-1)** similar in structure to adduct **4**. Frequency analysis and IRC following verify that **TS(4-1)** is a real transition state with $\nu = 401.1$ i cm⁻¹ and connects adduct **4** and dissociation product N₂ + CuCH₂, **1**. In **TS(4-1)** the C-N bond is stretched to 1.87 Å (B3LYP/II) and is nearly broken. The Cu-C distance decreases a little from 1.95 Å in adduct **4** to 1.91 Å, closer to the product CuCH₂. The N-N group rotates about 10° from adduct **4**, and the C-N-N angle becomes 123.9°. The barrier height is about 5.7 and 4.9 kcal/mol at the B3LYP/II and BLYP/II levels, respectively, and decreases to 2.9 kcal/mol at the CCSD(T)/II//B3LYP/II level. It seems that both DFT methods overestimate the barrier height. At the PCI-80/III//B3LYP/II level the barrier is 1.4 kcal/mol without zero-point energy correction (ZPC) and disappears after the zero-point energy is taken into account. This suggests that the stability of the adduct **4** in gas phase is on the borderline, too close to predict even with the present calculation. In the nitrogen matrix, where the matrix can stabilize the adduct by a few kilocalories per mole, the adduct **4** may be observed. The present finding is in agreement with the experiment that the production of CuCH₂ from Cu + N₂CH₂ takes place spontaneously at low temperature (12 K) in matrix. There is no direct path between the adduct **2** and the dissociation product N₂ + CuCH₂, **1**.

The adduct complexes Cu(N₂CH₂), **2** and **4**, can in principle be converted directly to the insertion product N₂(CuCH₂). Despite a substantial effort, we did not find such a transition

state. Several transition state search tries with different starting geometries either led to dissociation of the adduct to N_2 and $CuCH_2$ or converged to **TS(4-1)**. Therefore we conclude that the dinitrogen complex $N_2(CuCH_2)$ cannot be produced via unimolecular insertion reaction from the adduct. Instead, they can be formed only by exothermic and nearly barrierless dissociation of the adduct **4** to N_2 and $CuCH_2$, **1**, as just discussed above, which is then followed by the recombination reaction between these two products, N_2 and $CuCH_2$, in the matrix.

We did not find any transition state **TS(2-4)** connecting directly adduct **2** and **4**. Transition state search usually led to dissociation of the adduct to N_2 and $CuCH_2$. We also fixed the distance between the copper atom and the terminal N atom at various values, and the other degrees of freedom are optimized without symmetry constraint. The energies are quite high along the path, approximately 20 kcal/mol above that of adduct **2**. Thus we conclude that there is no low-lying transition state for the conversion from adduct **2** and **4**. Since the adduct **2** is not much lower than the reactants (-7.4 kcal/mol at the PCI/III/B3LYP/II level), adduct **2** may be easily converted to adduct **4** through dissociation.

B. Structure and Stability of the Product $CuCH_2$. Dissociation of complex **4**, $Cu \cdot CH_2N_2$, leads without barrier to the products **1**, $CuCH_2$, and N_2 . As seen in the Tables 1 and 2, the ground state of $CuCH_2$ is calculated to be 2B_1 with the Cu-C bond length of 1.87 Å and a Cu-CH₂ binding energy of 47.6 kcal/mol relative to the dissociation limit Cu (2S , s^1d^{10}) + CH₂ (3B_1) at the MP2/II level. DFT geometries are, in general, close to MP2 geometries, as shown in Table 1. The Cu-C bond is slightly (≤ 0.04 Å) shorter than MP2 results, especially more so using BLYP. The binding energy seems to be overestimated especially for BLYP (70.4 kcal/mol with basis set II). The CCSD(T)/II/B3LYP/II binding energy is 52.8 kcal/mol. The PCI-80/III/B3LYP/II method gives a binding energy of 63.7 kcal/mol, coincidentally the same as the value obtained using the B3LYP/II approximation. All *ab initio* methods including CCSD(T) underestimate the binding energy mainly due to limitation in the basis set. The PCI-80 estimate of the Cu-C bond strength is 61.4 kcal/mol including ZPC. No experimental result is known. These results are in good agreement with previous theoretical studies.¹⁹ Planelles's CIPSI study^{19a} gives the binding energy of 55.2 kcal/mol with the Cu-C distance of 1.82 Å, and Yamamoto's CASSCF-MR-CI study^{19b} gives the binding energy of 51.0 kcal/mol with the Cu-C distance of 1.932 Å. Large differences in the Cu-C distance between these studies may be caused in part by the frozen CH₂ structure^{19a} and nonanalytical optimization.^{19b}

As seen from Table 3, Mulliken population analysis indicates that the 2B_1 ground state of $CuCH_2$ arises from the interaction of Cu (2S , s^1d^{10}) and CH₂ (3B_1). The unpaired electron is mainly localized on the carbon atom. The atomic charge, $Cu^{+0.17}C^{-0.40}$, implies some ionic character in the Cu-C bond. However, a large overlap population of 0.41 between Cu and C indicates a substantial covalent component as well.

C. Structure and Stability of Dinitrogen Copper Complex $(N_2)CuCH_2$. Recombination of N_2 to $CuCH_2$ gives the dinitrogen copper complex $(N_2)CuCH_2$, which may have three different structures, **5-7**. Before discussing these structures, we should note that side-on coordination of N_2 in transition metal complexes in general is less favorable than end-on coordination.²⁰ In the side-on structure $[M](\eta^2-N_2)$, the interaction is a result of π -back-donation of electron density from an occupied metal d_{π} -orbital to the antibonding π^* orbital of N_2 , which weakens the N-N bond. In the end-on structure $[M](\eta^1-$

$N_2)$, the interaction is a result of donation of electron density from the σ -lone pair orbital of the bridged N atom to an empty σ -orbital of M, and therefore the N-N bond is not affected much.

The optimized geometries of structures **5-7** are found to be dependent on basis sets and electron correlation. Though no results of UHF or small basis set I are shown in Table 1, it was found that the inclusion of electron correlation at the MP2 level shortens the Cu-N bond by about 0.2 Å in the end-on structure **5** and nearly 1.0 Å in the side-on structures **6** and **7**. Improvement of the basis set from I to II shortens the Cu-N bond by an additional 0.2-0.4 Å.

The MP2/II and DFT/II optimized geometries given in Table 1 show that the Cu-C bonds are very similar in the three structures **5**, **6**, and **7**. On the other hand, the Cu-N distance in the end-on complex **5**, 1.92 Å (MP2/II), is much shorter than those in the two side-on structures, 2.20 Å in **6** and 2.26 Å in **7**. Obviously, N_2 interacts with $CuCH_2$ more strongly in the end-on case. The N-N distance in the side-on structures, 1.14 Å for both **6** and **7**, for instance, in MP2/II, is a little longer than that in the end-on complex, **5**, 1.10 Å. These results are in good agreement with the above-mentioned bonding picture.

Frequency analysis confirms that the end-on complex **5** is a minimum. Characterization of the complex **6** and **7**, however, varies with the basis set. With basis set I, both compounds **6** and **7** have one imaginary frequency mode corresponding to the tilting motion of N-N from the side-on toward the end-on structure. Using basis set II, complex **6** became a local minimum, while two imaginary frequencies appeared in complex **7**, with the additional one corresponding to H-H rotation around the Cu-C axis. This basis set dependency is probably caused by the weak nature of the interaction between N_2 and $CuCH_2$. Connecting the two minima **5** and **6**, the transition state **TS(6-5)** (so named because this is closer to **6** than to **5**) in Figure 2 was found to be only 0.6 kcal/mol higher than **6** at the MP2/II level without zero-point energy correction, as shown in Table 2. The barrier disappears after zero-point energy is taken into account. Therefore, we conclude that the side-on complex is not kinetically stable and cannot exist. It is not surprising that no vibrational spectrum corresponding to **6** was observed in the experiment.¹⁰

The end-on structure **5** is calculated to be 19.0 and 47.2 kcal/mol more stable relative to $N_2 + CuCH_2$ and $Cu + N_2CH_2$ dissociation limits, respectively, at the CCSD(T)/II/B3LYP/II level. The structures **6** and **7**, very close in energy with 0.7 kcal/mol difference, are 13.0 kcal/mol higher than the end-on complex **5** at the same level of theory. The PCI-80/III/B3LYP/II method (including relativistic correction and ZPC) gives the structure **5** to be 19.4 and 54.3 kcal/mol more stable relative to $N_2 + CuCH_2$ and $Cu + N_2CH_2$ dissociation limits. As seen in Table 2, DFT results are close to the *ab initio* results.

From the above discussions we may draw the following conclusions about the reaction energetics and the structures and stabilities of various intermediates, using the PCI-80 + relativistic correction + ZPC energies.

(i) The ground state reaction $Cu + CH_2N_2 \rightarrow CuCH_2 + N_2$ is exothermic by 35.4 kcal/mol and occurs without barrier, which is in good agreement with the experiment.

(ii) The dinitrogen complexes, $(N_2)CuCH_2$, cannot be formed directly from $Cu + CH_2N_2$ but can be formed only via recombination of dissociation products: $CuCH_2 + N_2$. It exists as structure **5**, where the N_2 molecule coordinates end-on to Cu of $CuCH_2$ and the bonding energy is 19.4 kcal/mol relative to the $N_2 + CuCH_2$ dissociation limit.

TABLE 4: Calculated Normal and Experimental Frequencies for CuCH₂

normal mode	reduced mass ^a	frequencies (cm ⁻¹)			experiment ^c	intensity ^b B3LYP/I
		UHF/I (UHF/II)	MP2/I (MP2/II)	B3LYP/I (BLYP/I)		
CH ₂ s-str(a ₁)	1.05	3194.1 (3226.8)	3086.5 (3207.2)	3093.6 (3024.5)	2960.7	m
CH ₂ sci(a ₁)	1.13	1438.5 (1428.3)	1397.7 (1405.8)	1326.8 (1279.7)	1344.9	s
CuC str(a ₁)	5.23	540.7 (518.9)	567.4 (559.4)	592.0 (590.3)	<i>614.0</i>	w
CH ₂ wag(b ₁)	1.27	515.6 (516.1)	474.9 (441.7)	437.2 (363.6)	526.0	m
CH ₂ a-str(b ₂)	1.12	3297.5 (3320.1)	3201.1 (3310.1)	3223.2 (3163.1)	3034.7	w
CH ₂ rock(b ₂)	1.17	595.7 (594.2)	576.5 (570.3)	632.4 (630.5)	573.2	m

^a The reduced mass for the specific normal mode, in amu. ^b We use the notation s (strong), m (middle), and w (weak) according to the calculated IR intensity: s, >100 km/mol; m, 10–100 km/mol; w, <10 km/mol. ^c Taken from ref 10. Assignment of the numbers in italic might be reversed, as discussed in text.

TABLE 5: Calculated Normal and Experimental Frequencies for End-on N₂CuCH₂ 5

normal mode	reduced mass ^a	frequencies (cm ⁻¹)				intensity ^b B3LYP/II
		UHF/I	MP2/II	B3LYP/II	experimental	
CH ₂ s-str(a ₁)	1.05	3178.1	3198.1	3096.5	2943.1	m
N≡N str(a ₁)	13.99	2619.2	3850.9 ^c	2379.1	2293.7	s
CH ₂ sci(a ₁)	1.13	1489.8	1435.3	1384.1	1366.6	w
CuC str(a ₁)	5.37	597.5	628.8	615.2	613.0	m
CH ₂ wag(b ₁)	1.30	567.0	561.9	580.9	569.1	m
CH ₂ a-str(b ₂)	1.05	3263.7	3283.6	3180.9	3002.9	m
CH ₂ rock(b ₂)	1.25	577.2	577.3	605.4	590.6	m

^a The reduced mass for the specific normal mode, in amu. ^b See footnote b of Table 4 for notation of IR intensity. ^c Large error due to spin contamination. See text.

It is worth mentioning that B3LYP energies agree quite well with these PCI-80 energies, with only serious exceptions of the dissociation limit N₂ + CuCH₂ **1** and **TS(4–1)**.

D. Vibrational Spectra of Intermediates. *Ab initio* and DFT calculated normal frequencies for CuCH₂ shown in Table 4 are in reasonable agreement with experiment, except for the assignment of two low frequencies. Plot of the normal modes (not shown) confirmed that 592.0 cm⁻¹ (a₁) is CuC stretch and 632.4 cm⁻¹ (b₂) is CH₂ rock. Therefore, we feel that the experimental assignment of 614.0 and 573.2 cm⁻¹ might be reversed. As expected, most of the calculated normal frequencies are larger than experimental fundamental frequencies because of the anharmonicity in the latter. Large deviations are found for low-frequency rocking and wagging modes, because of large quartic anharmonicities. It has been documented that both *ab initio* and DFT calculations are poor for low frequencies in CH₂ and CH₃ radicals where anharmonicity is extremely pronounced.²¹ When the lowest one is excluded and the next two are reversed, the average error in the calculated frequencies is 6%, 4%, 4%, and 4% at the UHF/I, MP2/I, BLYP/I, and B3LYP/I levels, respectively. B3LYP and MP2 frequencies are very similar and agree well with experiments excluding the exceptions above. Improvement of the basis set does not change UHF or DFT results but actually makes MP2 frequencies a little worse. It should be noticed that the analytical frequency calculation at DFT levels is four times faster than at MP2 level.

Calculated frequencies for the structure **5** (N₂)CuCH₂, shown in Table 5, are in reasonable agreement with experimental results, with the average error of 8% and 6% at the UHF and MP2 levels, respectively, excluding the N–N stretch. The N–N stretch frequency is poor for both methods; it is 14% and 70% larger than the experimental value, 2293.7 cm⁻¹, at the UHF and MP2 levels, respectively. Numerical calculation confirmed that it was not due to the second-derivative program. It is caused by the large effect of spin contamination on the MP2 frequency calculation. Documented as a serious problem in literature, presence of even a small amount of spin contamination in the UHF wave function can cause significant errors in calculated vibration frequencies at the UMP2 level.²² The magnitude of

TABLE 6: Vibrational Frequencies for CH₂N₂

normal mode	frequencies (cm ⁻¹)	
	B3LYP/II	experimental
C–N–N bend (b ₂)	424.7	
CH ₂ wag (b ₁)	440.1	427.2
C–N–N bend (b ₁)	582.9	
CH ₂ rock (b ₂)	1118.0	
C–N str (a ₁)	1228.5	1406.0
CH ₂ sci (a ₁)	1453.6	1169.6
N–N str (a ₁)	2226.3	2096.5
CH ₂ s-str (a ₁)	3206.6	3068.4
CH ₂ a-str (b ₂)	3329.1	

the error is not related to the degree of spin contamination, as measured by $\langle S^2 \rangle$, but to the geometrical derivative of $\langle S^2 \rangle$.²² Though other methods such as AUMP2²² could be used to improve the frequency, it is not the purpose of the present paper. DFT results with less spin contamination once again show advantages over MP2 and give very good agreement with experiment, with an average error of 4%.

For calibration and completeness, we presented in Table 6 the vibrational frequencies of the reactant CH₂N₂ at the B3LYP/II level and experimental values in ref 10. The agreement is quite good again, with an average error of 4%. As seen in the table, we feel that the assignment of CH₂ scissor and C=N stretch ought to be reversed in the experimental work. A similar isotope behavior of the two bands might have caused this difficulty.¹⁰ From the above comparison with experimental work, we can clearly see that *ab initio* and DFT methods give reliable vibrational frequencies for the present system. With a theoretical approach one can assign normal coordinates without ambiguity.

Feeling confident in our calculation, we next discuss the two adducts Cu(CH₂N₂) observed in the experiment with unknown structure in the N₂ matrix. They are labeled as adducts A and B according to the difference in their vibrational spectra under photolysis conditions.¹⁰ However, no information about the structures of adduct A and B is derived from the experiment. According to our calculation, two adducts, **2** and **4**, exist as shallow minima on the potential energy surface. Clearly they are candidates for the observed adducts, and their identity as A or B may be clarified by comparing the theoretical and experimental vibrational frequencies. Calculated normal frequencies and assignments of normal modes of the adducts **2** and **4** calculated at the B3LYP/II level are shown in Table 7, along with observed experimental vibrational frequencies of adducts A and B. It is clear that calculated frequencies of adduct **4** are in close agreement with the observed ones of adduct B, except for the N–N stretch frequency. Thus we assign adduct **4** as the adduct B observed in the experiment. The calculated N–N stretch frequency 1962.3 cm⁻¹ for **4** is smaller than the corresponding frequency 2226.3 cm⁻¹ of free CH₂N₂, which is expected from the weakening of the NN bond by interaction of CH₂N₂ with Cu. On the other hand, the experimental value

TABLE 7: Vibrational Frequencies for Adducts Cu(N₂CH₂)^a

theoretical			theoretical			experimental	
adduct 2			adduct 4			A	B
frequencies	normal mode	intensity ^b	frequencies	normal mode	intensity ^b	frequencies	frequencies
357.9	C–N–N bend (a')	m	513.3	Cu–C str (a')	m		
531.7	C–N–N bend (a'')	m	568.5	CH ₂ rock (a'')	m		
594.2	CH ₂ wag (a')	m	755.2	C–N str (a')	m	719.8	767.5
1100.0	CH ₂ rock (a')	m	1130.1	CH ₂ wag (a')	m		
1209.5	C–N str (a')	s	1166.1	CH ₂ rock (a'')	m	1209.5	1127.4
1468.6	CH ₂ sci (a')	w	1440.1	CH ₂ sci (a')	m	1571.9	1486.9
2048.0	N–N str (a')	s	1962.3	N–N str (a')	s		2196.8
3154.1	CH ₂ s-str (a')	m	3082.8	CH ₂ s-str (a')	w		2926.0
3263.5	CH ₂ a-str (a')	w	3139.6	CH ₂ a-str (a')	w		

^a Parameters of adduct 2 and 4 are from B3LYP/II in this work; those for A and B are from experiment in ref 10. ^b See footnote b of Table 4 for notation of IR intensity.

2196.8 cm⁻¹ attributed to this mode of the adduct is larger than the well-established value 2096.5 cm⁻¹ of free CH₂N₂, a somewhat unexpected result which needs to be studied further.

The agreement between the calculated frequencies of adduct 2 and the observed frequencies of adduct A is poorer, especially for the low frequency. A peak at 719.8 cm⁻¹ is observed experimentally in the N₂ matrix, but the closest value in our calculation is only 594.2 cm⁻¹. The difference is certainly too large for the current level of calculation, but since no other structure was found in the present work, we tentatively assign adduct 2 as the observed species A in the experiment. One has to remember that the calculation was for isolated adduct, while the experiment has been performed in the N₂ matrix; the solvent effect may account for these discrepancies.

E. DFT-Based Recontraction of the Cu Basis Set. As mentioned earlier, there has been some concern about the appropriateness of using Hay–Wadt ECPs along with their associated valence basis sets in DFT studies. Although Russo, Martin, and Hay²³ have found that the ECPs themselves perform well in DFT calculations, they did claim that some erratic behavior was found using the associated valence basis sets. To examine the issue in the case of Cu, we followed their suggestion and carried out some calculations for CuCH₂ with recontracted Hay–Wadt primitives in basis set I¹⁸ based on the DFT atomic wave functions. A more systematic study on other transitional metals is planned for the future.

The procedure of generating new contraction coefficients is straightforward. We performed a restricted DFT calculations for the Cu atom (²S) using the uncontracted Hay–Wadt primitives. We then picked contraction coefficients on the basis of the obtained atomic orbital. The contraction scheme from the original HF contracted basis set,¹⁸ i.e. {5s5p5d}/[3s2p2d], was maintained for this recontracted basis set. In this study, we examined two different DFT reconstructions, one with the LDA (S-VWN) and the other with B3LYP atomic orbitals, respectively.

Using the two newly recontracted basis sets, we optimized the geometry and calculated the binding energy and vibrational frequencies for CuCH₂. The basis sets for CH₂ are the same as in basis set I, namely, D95V. The results are shown in Table 8. As can be clearly observed, results change rather little among the three basis sets: original Hay–Wadt, S-VWN recontracted, and B3LYP recontracted Hay–Wadt primitives. The differences in the equilibrium Cu–C distance and the Cu–C binding energy are within 0.002 Å and 0.6 kcal/mol, respectively. The vibrational frequencies are also similar, with differences usually within 10 cm⁻¹. An exception is for the lowest vibrational frequency, for which the difference between the original Hay–Wadt and DFT recontracted results is around 21 cm⁻¹. The

TABLE 8: Comparison of the Optimized Geometries, Cu–CH₂ Binding Energy (BE) and Vibrational Frequencies (in cm⁻¹) for CuCH₂ between the Hay–Wadt Basis Set and Two DFT Recontracted Basis Sets^a

	Hay-Wadt basis I	S-VWN recontracted	B3LYP recontracted	experiment ^b
Cu–C (Å)	1.875	1.877	1.875	
Cu–CH ₂ BE (kcal/mol)	63.1	62.5	62.9	
CH ₂ s-str (a ₁)	3093.6	3090.7	3091.9	2960.7
CH ₂ sci (a ₁)	1326.8	1319.9	1321.3	1344.9
Cu–C str (a ₁)	592.0	596.4	596.7	<i>614.0</i>
CH ₂ wag (b ₁)	437.2	416.2	416.6	526.0
CH ₂ a-str (b ₂)	3223.2	3223.7	3225.6	3034.7
CH ₂ rock (b ₂)	632.4	627.2	632.5	573.2

^a Two DFT contraction schemes of the Hay–Wadt primitives are discussed in the text. ^b Taken from ref 10. Assignment of the numbers in italic might be reversed, as in the footnote b of Table 4.

two DFT reconstructions gives very similar results, with the largest difference in vibrational frequencies of around 6 cm⁻¹.

Thus, according to the current study, the original Hay–Wadt valence basis set derived from the Hartree–Fock calculation can be used for DFT/ECP calculations as well, at least for the case of copper. A more systematic study on the transition metals is planned for the near future.

V. Concluding Remarks

As we clearly see from the two applications, the analytical second derivative for ECP is very useful in the study of systems containing heavy atoms. One can easily identify the nature of a stationary point structure as a local minimum or a transition state, an essential ingredient for study of potential energy surfaces for chemical reactions, in particular, for complicated compounds containing transition metals. In addition, normal coordinate analysis is a very convenient tool for assignment of unidentified species. The availability of the ECP analytical second derivative for MP2 and DFT methods, not just for the HF method, is very important, as geometry optimization including electron correlation is becoming necessary and more popular. We hope that the present program will be made available to users in the near future as a part of the Gaussian package.

Acknowledgment. The authors thank Andy Komornicki, Russ Pitzer, Shigeru Obara, Joachim Werner, H. Stoll, and Chizuru Muguruma for discussions and assistance. The present research is in part supported by a grant from the National Science Foundation (CHE-9409020). The Phillips Petroleum Company Graduate Fellowship to Q.C. is also acknowledged. M.S. acknowledges Fellowship from the Swedish Natural Science Research Council.

References and Notes

- (1) See, for example: (a) Kahn, L. R.; Baybutt, P.; Truhlar, D. G. *J. Chem. Phys.* **1976**, *65*, 3826. (b) Kahn, L. R.; Hay, P. J.; Cowan, R. D. *J. Chem. Phys.* **1978**, *68*, 2386. (c) Stevens, W. J.; Basch, H.; Krauss, M. *J. Chem. Phys.* **1984**, *81*, 6026. (d) Krauss, M.; Stevens, W. J. *Annu. Rev. Phys. Chem.* **1984**, *35*, 357. (e) Hay, P. J.; Wadt, W. R. *J. Chem. Phys.* **1985**, *82*, 270. (f) Hay, P. J.; Wadt, W. R. *J. Chem. Phys.* **1985**, *82*, 284. (g) Hay, P. J.; Wadt, W. R. *J. Chem. Phys.* **1985**, *82*, 299.
- (2) Kitaura, K.; Obara, S.; Morokuma, K. *Chem. Phys. Lett.* **1981**, *77*, 452.
- (3) Breidung, J.; Thiel, W.; Komornicki, A. *Chem. Phys. Lett.* **1988**, *153*, 76.
- (4) Russo, T. V.; Martin, L. M.; Hay, P. J.; Rappe, A. K. *J. Chem. Phys.* **1995**, *102*, 9315.
- (5) (a) Frisch, M. J.; Trucks, G. W.; Schlegel, H. B.; Gill, P. M. W.; Johnson, B. G.; Wong, M. W.; Foresman, J. B.; Robb, M. A.; Head-Gordon, M.; Replogle, E. S.; Gomperts, R.; Andres, J. L.; Raghavachari, K.; Binkley, J. S.; Gonzalez, C.; Martin, R. L.; Fox, D. J.; Defrees, D. J.; Baker, J.; Stewart, J. J. P.; Pople, J. A. *Gaussian 92/DFT, Revision G.2*; Gaussian, Inc.: Pittsburgh, PA, 1993. (b) Frisch, M. J.; Trucks, G. W.; Schlegel, H. B.; Gill, P. M. W.; Johnson, B. G.; Robb, M. A.; Cheeseman, J. R.; Keith, T.; Petersson, G. A.; Montgomery, J. A.; Raghavachari, K.; Al-Laham, M. A.; Zakrzewski, V. G.; Ortiz, J. V.; Foresman, J. B.; Cioslowski, J.; Stefanov, B. B.; Nanayakkara, A.; Challacombe, M.; Peng, C. Y.; Ayala, P. Y.; Chen, W.; Wong, M. W.; Andres, J. L.; Replogle, E. S.; Gomperts, R.; Martin, R. L.; Fox, D. J.; Binkley, J. S.; Defrees, D. J.; Baker, J.; Stewart, J. P.; Head-Gordon, M.; Gonzalez, C.; Pople, J. A. *Gaussian 94, Revision A.1*; Gaussian, Inc.: Pittsburgh PA, 1995.
- (6) McMurchie, L. E.; Davison, E. R. *J. Comput. Phys.* **1981**, *44*, 289.
- (7) Stoll, H. Private communication.
- (8) Pitzer, R. M. *Int. J. Quantum Chem.* **1991**, *40*, 773.
- (9) Koga, N.; Morokuma, K. *J. Mol. Struct.: THEOCHEM* **1993**, *300*, 181.
- (10) Chang, S. C.; Kafafi, Z. H.; Hauge, R. H.; Billups, W. E.; Margrave, J. L. *J. Am. Chem. Soc.* **1987**, *109*, 4508.
- (11) Moore, C. E. *Atomic Energy Levels*; NSRD-NBS; U.S. Government Printing Office: Washington, DC, 1971; Vols. II and III.
- (12) Boldyrev, A. I.; Schleyer, P. v. R.; Higgins, D.; Thomson, C.; Kramarenko, S. S. *J. Comput. Chem.* **1992**, *13*, 1067.
- (13) (a) Becke, A. D. *Phys. Rev. A* **1988**, *38*, 3098. (b) Becke, A. D. *J. Chem. Phys.* **1992**, *96*, 2155.
- (14) Becke, A. D. *J. Chem. Phys.* **1993**, *98*, 5648.
- (15) Lee, C.; Yang, W.; Parr, R. G. *Phys. Rev. B* **1988**, *37*, 785.
- (16) (a) Siegbahn, P. E. M.; Blomberg, M. R. A.; Svensson, M. *Chem. Phys. Lett.* **1994**, *35*, 223. (b) Siegbahn, P. E. M.; Svensson, M.; Boussard, P. J. E. *J. Chem. Phys.* **1995**, *102*, 5377.
- (17) Chong, D. P.; Langhoff, S. R. *J. Chem. Phys.* **1986**, *84*, 5606.
- (18) (a) Dunning, T. H.; Hay, P. J. *Modern Theoretical Chemistry*; Plenum: New York, 1976. (b) Hehre, W. J.; Ditchfield, R.; Pople, J. A. *J. Chem. Phys.* **1972**, *56*, 2257. (c) Hariharan, P. C.; Pople, J. A. *Theor. Chim. Acta* **1973**, *28*, 213. (d) Gordon, M. S. *Chem. Phys. Lett.* **1980**, *76*, 163. (e) Wachters, A. J. H. *J. Chem. Phys.* **1970**, *52*, 1033. (f) Huzinaga, S. *J. Chem. Phys.* **1965**, *42*, 1293.
- (19) (a) Planelles, J.; Merchan, M.; Tomas, F. *Chem. Phys. Lett.* **1988**, *149*, 222. (b) Mochizuki, Y.; Tanaka, K.; Ohno, K.; Tatewaki, H.; Yamamoto, S. *Chem. Phys. Lett.* **1988**, *152*, 457.
- (20) (a) Sakaki, S.; Morokuma, K.; Ohkubo, K. *J. Am. Chem. Soc.* **1985**, *107*, 2686. (b) Musaev, D. G. *Russ. J. Inorg. Chem.* **1988**, *33*, 1853. (c) Yamabe, T.; Hori, K.; Minato, T.; Fukui, K. *Inorg. Chem.* **1980**, *80*, 2154. (d) Siegbahn, P. E. M.; Blomberg, M. R. A. *Chem. Phys.* **1984**, *87*, 189.
- (21) See, for example: Johnson, B. G.; Gill, P. M. W.; Pople, J. A. *J. Chem. Phys.* **1993**, *98*, 5612.
- (22) Jensen, F. *Chem. Phys. Lett.* **1990**, *169*, 519.
- (23) Russo, T. V.; Martin, R. L.; Hay, P. J. *J. Phys. Chem.* **1995**, *99*, 17085.

JP960554H